

# An Advanced Model of Designing Controlled Strain Rate Dies for Axisymmetric Extrusion

Y.H. Lu and S.W. Lo

(Submitted 6 August 1997; in revised form 6 July 1998)

This paper presents an advanced model for the design of stream-lined axisymmetric extrusion dies based on a prescribed strain rate variation. This is vital to the preparation of the workpieces with mechanical properties that are very sensitive to the strain rate distribution during a manufacturing process. The proposed model, which incorporates Tresca's yield criterion and velocity field with the die angularity, can give an accurate prediction of the die shape. Influences of the interfacial friction and the ram velocity on the die geometry are also studied. As a verification of the proposed model, an updated Lagrangian formulated, elasto-plastic finite element program was developed to analyze the axisymmetric extrusion process. A clear derivation of the load-correction matrix, which is indispensable for the surface traction rate equilibrium in the updated Lagrangian formulation, is described for the application of the finite element simulation. A friction-correction matrix based on a constant shear law is used to solve the interfacial friction. From the comparison of the resultant strain rate distribution, it verifies that the advanced model can determine the surface angularity and friction force in the extrusion process.

**Keywords** advanced model, axisymmetric extrusion, constant strain rate

## 1. Introduction

Most materials can be manufactured via extrusion process for producing shaped products. However, extrusion technology has undergone limited improvement in recent years due to the inherent complexity of the process. Especially for some composite materials, the strain rate variation experienced in the material as it flows through the die is an important factor in the extrusion process. The strain rate must be controlled under a certain magnitude so that the influences of the generation and transfer of heat, as well as the distortion of the material on the metallurgical variations, are acceptable.

Conventional extrusion dies, such as the flat face (shear) dies and converging dies, have been used in the extrusion for several decades. Because of the hot shortness resulting from considerable adiabatic shear heating, the shear dies can only be operated at low ram speeds. Conversely, converging dies, which have conical, parabolic, or streamlined shapes, are better suited to generate smoother material flow. According to the study carried out by Srinivasan et al. (Ref 1), when conical dies are applied, the flowing material is subjected to rigid body rotations and abrupt changes in velocity at the entrance and exit planes of the die. This yields great redundant work. The situation of a parabolic die is similar. As for streamlined dies, such as cubic spline dies, the material flow path is smooth and the velocity is continuous, but the strain rate generally peaks toward the exit (Ref 1). Obviously, a new technique of developing adequate shapes for controlling strain rate is necessary in the extrusion process.

**Y.H. Lu**, National I-Lan Institute of Agriculture and Technology, Department of Mechanical Engineering, 1 Shen-Lung Road, I-Lan, Taiwan, 260, R.O.C.; and **S.W. Lo**, National Yunlin University of Science and Technology, Department of Mechanical Engineering, Touliu, Yunlin, Taiwan, 640, R.O.C. Contact Y.H. Lu at e-mail yhlu@cmail.niiat.edu.tw.

Srinivasan et al. (Ref 1) developed an ideal work slab method to predict a die profile, which can have a controlled strain rate in extrusion. However, their methodology ignores the influences of surface angularity and interfacial friction force on the material flow. Hence it cannot apply to the processes with high friction stress and sloped tool-workpiece contacted surface. Chang (Ref 2) recently proposed a new advanced slab method, which combines the velocity fields with the yield criterion, for plane strain strip rolling process. In Chang's method, Mohr's circle is used so the stress state can involve the effects of the surface angularity and friction force. In this paper, Chang's method will be modified and applied to the design of strain rate driven dies for the axisymmetric extrusion process.

As a verification for the developed advanced slab method, an updated Lagrangian formulated, elasto-plastic finite element program was also constructed to analyze the axisymmetric extrusion process. Due to the change of the configuration of the tool-workpiece surface, the equilibrium of the surface traction rate induced the load-correction matrix (Ref 3, 4). The theoretical formulation of the load-correction matrix for axisymmetric process was derived in this work. Thereafter, the friction-correction matrix of constant friction shear law was derived to solve the frictional traction force rate. After incorporating these two correction matrices into the usual updated Lagrangian formulated, finite element analysis, the axisymmetric extrusion was simulated completely from the initial nonsteady state to the steady state. The resultant strain rate distribution of the advanced model varies so that it can be applied to solve the surface angularity and friction force.

## 2. Theory

### 2.1 Advanced Slab Model

As shown in Fig. 1, the material is pushing through a convergent axisymmetric die with the inlet diameter  $h_1$  and the out-

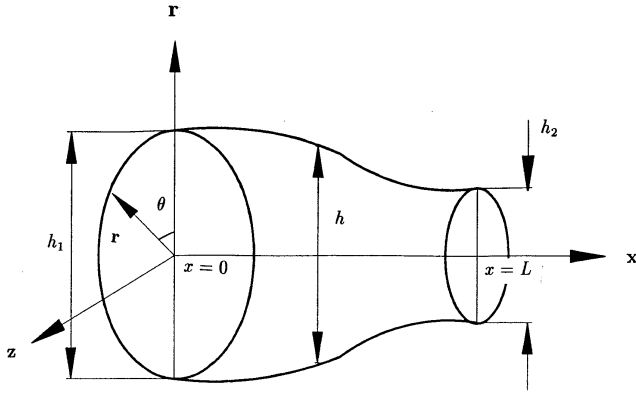


Fig. 1 Schematic representations of axisymmetric extrusion

let diameter  $h_2$ . The length of the die is  $L$ . If the material undergoes a prescribed strain rate, it is convenient to use the Mohr's circle technique to describe the shear stress distribution including angularity effect. Knowing that the state of stresses at any point under plastic deformation satisfies the Tresca yield criterion, the radius of this Mohr's circle equals the shear yield strength of the workpiece, say  $k$ . It is written as

$$(\sigma_x - \sigma_r)^2 + 4\tau_{xr}^2 = 4k^2 \quad (\text{Eq 1})$$

In the constant friction law, the shear stress along the tool-workpiece interface can be expressed as

$$\tau = -mk \quad (\text{Eq 2})$$

where  $m$  is the friction factor. If the friction angle,  $\alpha$ , is defined as

$$\alpha = \sin^{-1}(-mu) \quad (\text{Eq 3})$$

then the shear stress on the tool-workpiece interface with respect to the  $x$ - $r$  coordinate system is obtained geometrically from Mohr's circle

$$\tau_{xr}(x, h/2) = k \sin(\alpha + 2\lambda) \quad (\text{Eq 4})$$

where  $\lambda$  represents the geometrical angularity of process. That is

$$\lambda = \tan^{-1} \left( \frac{1}{2} \frac{dh}{dx} \right) \quad (\text{Eq 5})$$

Because the shear stress  $\tau_{xr}$  vanishes at the centerline of the workpiece, it is assumed that the shear stress varies linearly along the thickness of the workpiece and can be expressed as

$$\tau_{xr}(x, r) = (2kr \sin \phi) / h \quad (\text{Eq 6})$$

where

$$\phi = \alpha + 2\lambda \quad (\text{Eq 7})$$

After substituting Eq 6 into Eq 1, the following equation is obtained:

$$\sigma_x - \sigma_r = 2k \sqrt{1 - \left( \sin \phi \frac{2r}{h} \right)^2} \quad (\text{Eq 8})$$

According to the Levy-Mises flow, the relation of the strains rate to stresses is described as

$$\frac{\dot{\epsilon}_x - \dot{\epsilon}_r}{\dot{\epsilon}_{xr}} = \frac{\sigma_x - \sigma_r}{\tau_{xr}} \quad (\text{Eq 9})$$

Using the definition of strains rate to the velocity components, an equation that combines the velocity components to the stresses is derived as

$$\frac{\partial u}{\partial r} + \frac{\partial v}{\partial x} = -6 \frac{\partial v}{\partial r} \frac{\tau_{xr}}{\sigma_x - \sigma_r} \quad (\text{Eq 10})$$

where  $u$  and  $v$  are the velocity components in the global  $x$  and  $r$  coordinates. Moreover, it is assumed that the vertical component  $v$  varies linearly across the workpiece:

$$v(x, r) = \frac{u_s r}{h} \frac{dh}{dx} \quad (\text{Eq 11})$$

where  $u_s$  is the horizontal component of velocity on the tool-workpiece interface. Combining Eq 6, 8, and 11, the general expression of  $u$  can be derived to be

$$u(x, r) = \frac{1}{16} \left[ 1 - 8 \left( \frac{r}{h} \right)^2 \right] [u_s' h h' + u_s (h h'' - h'^2)] + \frac{3u_s h'}{2 \sin \phi} \left[ \sqrt{1 - \left( \frac{2r}{h} \sin \phi \right)^2} - C \right] + \frac{4q}{\pi h^2} \quad (\text{Eq 12})$$

where ' means the derivative with respect to  $x$  direction.  $q$  is the volume flow rate which is:

$$q = \pi \left( \frac{h_1}{2} \right)^2 u_r = \pi \left( \frac{h_1}{2} \right)^2 (u_1)_{\text{ave}} \quad (\text{Eq 13})$$

where  $u_r$  is the ram velocity, which equals the average entrance velocity  $(u_1)_{\text{ave}}$ .  $C$  is denoted as the inhomogeneity function and is derived as

$$C = \left( \frac{\sigma_x - \sigma_r}{2k} \right)_{\text{ave}} = \frac{8}{h^2} \int_0^{h/2} r \sqrt{1 - \left( \frac{2r}{h} \sin\phi \right)^2} dr = 2(1 - \cos^3\phi)/3\sin^2\phi \quad (\text{Eq 14})$$

Physically,  $C$  represents the total effect of surface angularity and friction force on the “average” yield criterion. It is assumed that the shear strain rate is relatively small with respect to the strains rate of  $x$  and  $r$  direction. Therefore, the strain rate of  $x$  and  $r$  will be the principal strain rate. Hence, the equivalent strain rate is derived as

$$\dot{\epsilon} = -2\dot{\epsilon}_r = -2 \frac{u_s h'}{h} \quad (\text{Eq 15})$$

It is found that the equivalent strain rate is a function of the horizontal velocity on the tool-workpiece interface. Substituting Eq 15 into Eq 12 and letting  $r$  be  $h/2$ :

$$\dot{\epsilon} u'_s = u_s \left\{ \dot{\epsilon}' - \frac{32^2}{h} \left[ u_s + \frac{3h\dot{\epsilon}}{4\sin\phi} (\cos\phi - C) - \frac{4q}{\pi h^2} \right] \right\} \quad \dot{\epsilon} \neq 0 \quad (\text{Eq 16})$$

If the strain rate is not zero, it is convenient to define the following nondimensional terms:

$$X = \frac{x}{L} \quad H = \frac{h}{L} \quad U_s = \frac{u_s}{u_r} \quad E = \frac{\dot{\epsilon} L}{u_r} \quad (\text{Eq 17})$$

and Eq 15 and 16 can be rewritten in nondimensional forms as:

$$H' = \frac{HE}{2U_s} \quad (\text{Eq 18})$$

and

$$U'_s = U_s \left\{ \frac{E'}{E} - \frac{32U_s}{H^2 E} \left[ U_s + \frac{3HE}{4\sin\phi} (\cos\phi - C) - \frac{H_1^2}{H^2} \right] \right\} \quad E \neq 0 \quad (\text{Eq 19})$$

It is noted that the nondimensional strain rate  $E$  actually gives the combined effect of the strain rate, die length, and the ram velocity.  $X$ ,  $H$ , and  $U_s$  represent the nondimensional position, diameter, and horizontal velocity, respectively.

As for the entrance and exit where the strain rate approaches zero, Eq 16 can be differentiated with respect to  $x$  again and applied to the condition of zero strain rate. The nondimensional form of the velocity gradient for zero strain rate is to be:

$$U'_s = \left[ \frac{H^2 E''}{32} - \frac{3HE'}{4\sin\phi} (\cos\phi - C) \right] \left( 2 - \frac{H_1^2}{H^2 U_s} \right)^{-1} \quad E = 0 \quad (\text{Eq 20})$$

From Eq 12, the surface velocity  $u_s$  at the position where  $h'$  vanishes, such as the entrance and the exit, is found to be

$$u_s = u_r h_1^2 / [h^2(1 + hh''/16)] = (u_1)_{\text{ave}} h_1 / h(1 + hh''/16) \quad (\text{Eq 21})$$

where  $(u_1)_{\text{ave}}$  is the average entrance velocity, which is equal to the ram speed,  $u_r$ . Because  $h''$  is usually negative at the entrance and positive at the exit, the surface velocity is faster than the average velocity at the entrance, while it is slower than the average velocity at the exit. For the sake of simplicity,  $h''$  is usually set to be zero, and the deformation is uniform at  $X = 0$  and  $X = 1$ . The ram velocity  $u_r$ , which is identical to  $(u_1)_{\text{ave}}$  can be just denoted as  $u_1$ .

The nondimensional variables  $H$  and  $U_s$  can be solved by integrating Eq 18 and 19, or 20, simultaneously with boundary condition  $H_1$  for the given values of  $E$  and friction factor  $m$ . The final thickness, say  $H_2$ , can be used to calculate the size reduction  $R^*$  and reduction  $R$ , which are defined as

$$R^* = \frac{h_1 - h_2}{h_1} \quad R = \frac{h_1^2 - h_2^2}{h_1^2} \quad (\text{Eq 22})$$

## 2.2 Finite Element Modeling Analysis

In the framework of the application of the incremental deformation for the metal forming process, it is convenient to adopt the updated Lagrangian formulation for the virtual work rate equation (Ref 5):

$$\int_v [\delta \dot{\epsilon}] \{s\} dv = \int_S [\delta v] \{f_0\} dS \quad (\text{Eq 23})$$

where  $\{s\}$  is the Lagrange stress rate,  $\{\dot{\epsilon}\}$  is the velocity gradient of  $\partial v_i / \partial x_j$ , and  $\{f_0\}$  is the rate of the nominal traction assigned over the surface,  $S$ , on the current configuration. Because the principal axes of the material element will be spun in the large forming process, it leads to adopting the Jaumann rate of Kirchhoff stress,  $\{\dot{t}^*\}$ , to relate to the Lagrange stress rate. The relation in the updated Lagrangian formulation is (Ref 5):

$$[\dot{s}] = \{\dot{t}^*\} - [\dot{\epsilon}][\sigma] - [\sigma][\dot{\epsilon}] + [\sigma][\dot{\epsilon}] \quad (\text{Eq 24})$$

where  $[\sigma]$  is the current Euler stress and  $[\dot{\epsilon}]$  represents the Euler strain rate. The relation between  $[\dot{\epsilon}]$  and  $\{\dot{\epsilon}\}$  is:

$$[\dot{\epsilon}] = \frac{1}{2} (\{\dot{\epsilon}\} + \{\dot{\epsilon}\}^T) \quad (\text{Eq 25})$$

Equation 24 can be written in a contracted form as

$$\{\dot{s}\} = \{\dot{t}^*\} + [D_g]\{\dot{e}\} \quad (\text{Eq 26})$$

Explicitly,  $[D_g]$  comprises the initial stress components at each deformation stage and is called the initial stress matrix.

It is natural to express the velocity,  $v$ , strain rate,  $\dot{\epsilon}$ , and velocity gradient,  $\dot{e}$ , in terms of the nodal velocity,  $\dot{d}$ , that is:

$$\begin{aligned} \{v\} &= [N]\{\dot{d}\} \\ \{\dot{\epsilon}\} &= [B_\epsilon]\{\dot{d}\} \\ \{\dot{e}\} &= [B_c]\{\dot{d}\} \end{aligned} \quad (\text{Eq 27})$$

where  $[N]$  is the shape function.  $[B_\epsilon]$  and  $[B_c]$  represent the strain rate-velocity matrix and velocity gradient-velocity matrix, respectively. Substituting Eq 26 and 27 into Eq 23, the discretized element stiffness matrix is evaluated to obtain the entire global stiffness matrix:

$$([K_{ep}] + [K_g])\{\dot{d}_g\} = \{\dot{F}_0\} \quad (\text{Eq 28})$$

where  $[K_{ep}]$  is the conventional elasto-plastic stiffness matrix.  $[K_g]$  represents the geometric stiffness matrix, which relates to the initial stress matrix  $[D_g]$ .  $\{\dot{d}_g\}$  is the nodal velocity in the global coordinate system.  $\{\dot{F}_0\}$  denotes the nominal force rate on the contacting surface. It is noted that the change of the configuration on the contacted surface,  $\{\dot{F}_0\}$  should be replaced by the true force rate  $\{\dot{F}\}$  and a load correction matrix  $[K_c]$ , which is related to local nodal velocity  $\{\dot{d}_g^S\}$ :

$$\{\dot{F}_0\} = \{\dot{F}\} + [K_c]\{\dot{d}_g^S\} \quad (\text{Eq 29})$$

where superscript  $S$  denotes the tool-workpiece contacted surface.

**Load-Correction Matrix.** As shown in Fig. 2, considering the term in the surface integral part of Eq 23 and referring it to the local coordinates  $\xi$ ,  $\eta$ , and  $\zeta$ , the authors have

$$\begin{aligned} \{\vec{f}\} &= f_{t1} \vec{t}_1 + f_{t2} \vec{t}_2 + f_n \vec{n} \\ \dot{\theta}_1 &= -\kappa_1 v_\zeta \\ \dot{\theta}_2 &= \kappa_2 v_\xi \end{aligned}$$

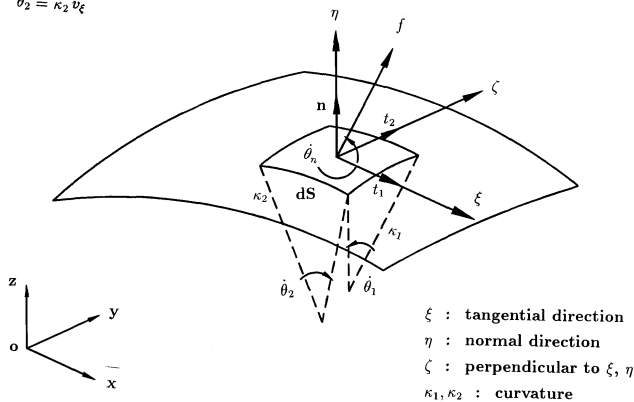


Fig. 2 Surface element and relation of local coordinate

$$\begin{aligned} \{f_0\}dS &= \frac{d}{dt} (\{f\}dS) = \dot{f}_{t1} \vec{t}_1 dS + \dot{f}_{t2} \vec{t}_2 dS + \dot{f}_n \vec{n} dS \\ &+ f_{t1} \dot{\vec{t}}_1 dS + f_{t2} \dot{\vec{t}}_2 dS + f_n \dot{\vec{n}} dS + f_{t1} \vec{t}_1 \dot{d}S + f_{t2} \vec{t}_2 \dot{d}S + f_n \vec{n} \dot{d}S \end{aligned} \quad (\text{Eq 30})$$

where  $t_1$ ,  $t_2$ , and  $n$  are the unit vectors, which are the tangential and normal directions of the surface. The relations of the unit vectors and their rates are as follows:

$$\dot{\vec{t}}_1 = -\dot{\theta}_2 \vec{n} + \dot{\theta}_n \vec{t}_2 \quad (\text{Eq 31})$$

$$\dot{\vec{t}}_2 = \dot{\theta}_1 \vec{n} - \dot{\theta}_n \vec{t}_1 \quad (\text{Eq 32})$$

$$\dot{\vec{n}} = \dot{\theta}_2 \vec{t}_1 - \dot{\theta}_1 \vec{t}_2 \quad (\text{Eq 33})$$

where  $\dot{\theta}_1$ ,  $\dot{\theta}_2$ ,  $\dot{\theta}_n$ , and their direction are shown in Fig. 2. By substituting unit vectors rates into Eq 30 and letting the unit vectors coincide with the local coordinate system:

$$\begin{aligned} \frac{d}{dt} (\{f\}dS) &= \left( \dot{f}_{t1} - \dot{f}_{t2} \dot{\theta}_n + \dot{f}_n \dot{\theta}_2 + f_{t1} \frac{dS}{dt} \right) \vec{t}_1 dS \\ &+ \left( \dot{f}_{t2} + \dot{f}_{t1} \dot{\theta}_n - \dot{f}_n \dot{\theta}_1 + f_{t2} \frac{dS}{dt} \right) \vec{t}_2 dS \\ &+ \left( \dot{f}_n - \dot{f}_{t1} \dot{\theta}_2 + \dot{f}_{t2} \dot{\theta}_1 + f_n \frac{dS}{dt} \right) \vec{n} dS \end{aligned} \quad (\text{Eq 34})$$

It is convenient to express the virtual velocity along the surface of the rigid tool as:

$$[\delta v] = [\delta v_\xi \quad \delta v_\zeta \quad \delta v_\eta] \quad (\text{Eq 35})$$

and

$$\begin{aligned} \int_S [\delta v] \{f_0\} dS &= \int_S [\delta v] \frac{d}{dt} (\{f\}dS) \\ &= \int_S \left[ \delta v_\xi \left( \dot{f}_{t1} - \dot{f}_{t2} \dot{\theta}_n + \dot{f}_n \dot{\theta}_2 + f_{t1} \frac{dS}{dt} \right) \right. \\ &+ \delta v_\zeta \left( \dot{f}_{t2} + \dot{f}_{t1} \dot{\theta}_n - \dot{f}_n \dot{\theta}_1 + f_{t2} \frac{dS}{dt} \right) \\ &+ \left. \delta v_\eta \left( \dot{f}_n - \dot{f}_{t1} \dot{\theta}_2 + \dot{f}_{t2} \dot{\theta}_1 + f_n \frac{dS}{dt} \right) \right] dS \end{aligned} \quad (\text{Eq 36})$$

The terms which contain  $f_n$ ,  $f_{t1}$ , and  $f_{t2}$  in Eq 36 will induce the load correction matrix  $[K_c]$ . If the geometric relation is incorporated in the contacted surface, it shows

$$\begin{aligned} \dot{\theta}_1 &= -\kappa_1 v_\zeta & \dot{\theta}_2 &= \kappa_2 v_\xi \\ \dot{\theta}_n &= \frac{1}{2} \left( \frac{\partial v_\zeta}{\partial \xi} - \frac{\partial v_\xi}{\partial \zeta} \right) \frac{dS}{dS} = \left( \frac{\partial v_\xi}{\partial \xi} + \frac{\partial v_\zeta}{\partial \zeta} \right) \end{aligned} \quad (\text{Eq 37})$$

where  $\kappa_1$  and  $\kappa_2$  are the curvatures of the tool surface. For the problem of axisymmetric process, it is natural that the following relations should be unconditionally satisfied as:

$$\begin{aligned} \delta v_\zeta &= 0 & f_{t2} &= 0 \\ v_\zeta &= 0 & \frac{\partial v_\zeta}{\partial \zeta} &= \frac{v_r}{r} \end{aligned} \quad (\text{Eq 38})$$

As shown in Fig. 3, the relation of the radial velocity component  $v_r$  is equal to  $-v_\xi \sin \alpha$ . Assuming that the tangential velocity,  $v_\xi$ , and normal velocity,  $v_\eta$ , are linearly distributed for the material element along the tool-workpiece interface, it will be possible to integrate along the elemental line to obtain the explicit load correction matrix  $[K_c]$  for the triangular element in Fig. 4:

$$[K_c] = \begin{bmatrix} -\frac{F_n \kappa_2}{3} + \frac{F_t}{2l} + \frac{F_t \sin \alpha}{3r} & 0 & -\frac{F_n \kappa_2}{6} - \frac{F_t}{2l} + \frac{F_n \sin \alpha}{6r} & 0 \\ \frac{F_t \kappa_2}{3} + \frac{F_n}{2l} + \frac{F_n \sin \alpha}{3r} & 0 & \frac{F_t \kappa_2}{6} - \frac{F_n}{2l} + \frac{F_n \sin \alpha}{6r} & 0 \\ -\frac{F_n \kappa_2}{6} + \frac{F_t}{2l} + \frac{F_t \sin \alpha}{6r} & 0 & -\frac{F_n \kappa_2}{3} - \frac{F_t}{2l} + \frac{F_t \sin \alpha}{3r} & 0 \\ \frac{F_t \kappa_2}{6} + \frac{F_n}{2l} + \frac{F_n \sin \alpha}{6r} & 0 & \frac{F_t \kappa_2}{3} - \frac{f_n}{2l} + \frac{F_n \sin \alpha}{3r} & 0 \end{bmatrix} \quad (\text{Eq 39})$$

where  $F_n$  and  $F_t$  are the known traction force components.  $l$  is the contacted length of the triangular element.

Substituting Eq 29 into Eq 28 and incorporating  $[K_c]$ , the finite element stiffness equation that connects the nodal velocity  $\{d_l^S\}$  on the tool-workpiece interface and the internal nodal velocity  $\{d_l^I\}$  is

$$\begin{bmatrix} K_{ep}^{SS} + K_g^{SS} + K_c & K_{ep}^{SI} + K_g^{SI} \\ K_{ep}^{IS} + K_g^{IS} & K_{ep}^{II} + K_g^{II} \end{bmatrix} \begin{Bmatrix} d_l^S \\ \vdots \\ d_l^I \end{Bmatrix} = \begin{Bmatrix} \dot{F}_t \\ \dot{F}_n \\ \vdots \\ 0 \end{Bmatrix} \quad (\text{Eq 40})$$

where  $\dot{F}_n$  is the normal force rate.  $\dot{F}_t$  is the friction force rate, which comes from the integral of the term  $f_{t1}$  in Eq 36.

**Friction-Correction Matrix.** The constant shear friction law is adopted to evaluate  $\dot{F}_t$  in this paper. The constitutive equation of the constant shear friction stress rate can be represented as (Ref 3):

$$\dot{f}_{t1} = \begin{cases} -\beta \Delta \dot{d}_\xi & \equiv \Sigma \Delta d_\xi \leq d_{above} \{ \Sigma \Delta d_\xi \text{ symbol} \\ 0 & \end{cases} \quad (\text{Eq 44})$$

where  $\Delta \dot{d}_\xi$  is the nodal relative velocity between tool and workpiece.  $\Sigma \Delta d_\xi$  is the summation of the nodal relative displacement

$\Delta d_\xi$ .  $\beta$  is equal to  $mk/d$ . Physically, the meaning of the constitutive equation is the friction stress, which will be equal to  $mk$  when the accumulated nodal relative displacement reaches the prescribed distance,  $d$ . Otherwise the friction stress will be linearly increased by the nodal relative displacement. Considering a triangular element on the tool, the nodal relative velocity  $\Delta \dot{d}_\xi$  is expressed as

$$\Delta \dot{d}_\xi = \left[ 1 - \frac{s}{l} \frac{s}{l} \right] \begin{Bmatrix} \Delta \dot{d}_{1\xi}^S \\ \Delta \dot{d}_{2\xi}^S \end{Bmatrix} \quad (\text{Eq 42})$$

Therefore, the  $\dot{F}_t$  can be evaluated by the following integral computation

$$\{F_t\} = \int_S \delta v_\xi \dot{f}_{t1} dS = [\delta d_{1\xi}^S \quad \delta d_{2\xi}^S] (-[K_f^{SS}]) \begin{Bmatrix} \Delta \dot{d}_{1\xi}^S \\ \Delta \dot{d}_{2\xi}^S \end{Bmatrix} \quad (\text{Eq 43})$$

where  $[K_f^{SS}]$  in Eq 43 represents the friction correction matrix:

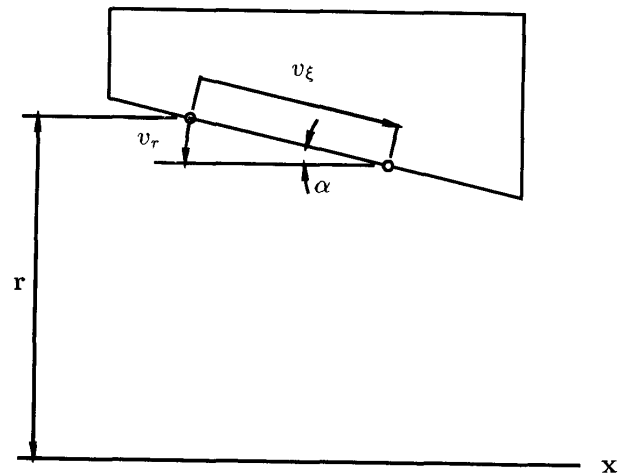


Fig. 3 The relation between velocities  $v_r$  and  $v_\xi$

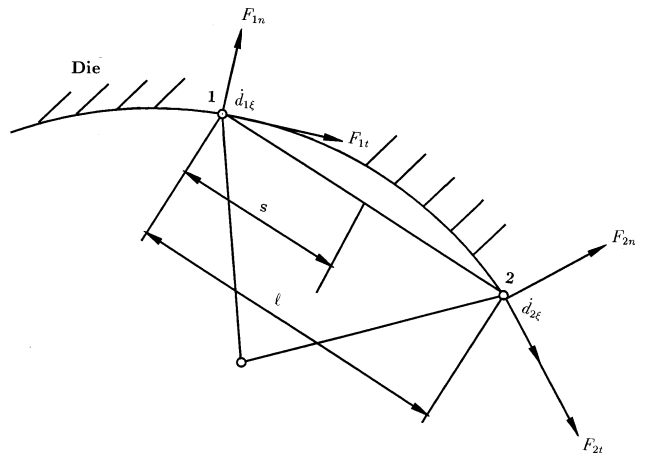


Fig. 4 Nodal forces and local velocities of a triangular element

(Eq 44)

As shown in Fig. 5, the tool or die has a specified velocity  $\dot{d}_D$  in a deformation stage.  $M$  is a contacted point on the tool surface. Hence, the nodal velocity of point  $M$  can be decomposed into the following form

$$\{\dot{d}_l^S\}_M = \begin{Bmatrix} \dot{d}_{D\xi} \\ \dot{d}_{D\eta} \end{Bmatrix} + \{\Delta\dot{d}_l^S\}_M \quad (\text{Eq 45})$$

The  $\dot{d}_{D\xi}$  and  $\dot{d}_{D\eta}$  are the tool velocities in the local coordinates. Substituting Eq 44 and 45 into Eq 40:

$$\begin{bmatrix} K_{ep}^{SS} + K_g^{SS} + K_c + K_I^{SS} & K_{ep}^{SI} + K_g^{SI} \\ K_{ep}^{IS} + K_g^{IS} & K_{ep}^{II} + K_g^{II} \end{bmatrix} \begin{Bmatrix} \Delta\dot{d}_l^S \\ \vdots \\ \dot{d}_g^I \end{Bmatrix} = \begin{Bmatrix} 0 \\ F_n \\ \vdots \\ 0 \end{Bmatrix} - \{\dot{F}_a\} \quad (\text{Eq 46})$$

$\{\dot{F}_a\}$  is the apparent force rate, which connects the tool velocity and has the form:

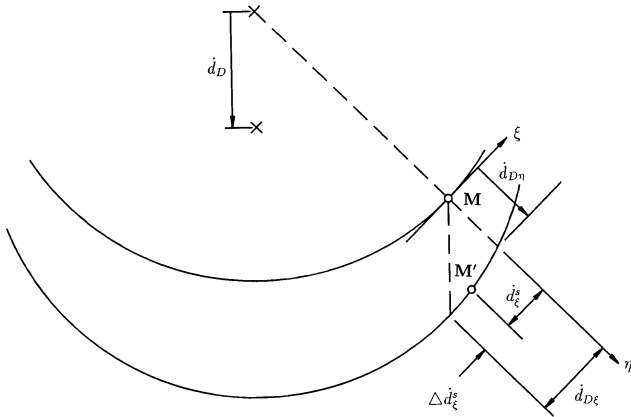


Fig. 5 The relation of tool velocity and nodal relative velocity

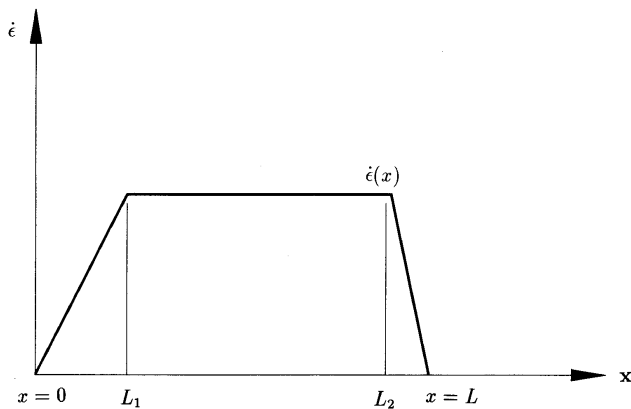


Fig. 6 Linear strain rate variation in special ideal work model

$$\{\dot{F}_a\} = \begin{bmatrix} K_{ep}^{SS} + K_g^{SS} + K_c & K_{ep}^{SI} + K_g^{SI} \\ K_{ep}^{IS} + K_g^{IS} & K_{ep}^{II} + K_g^{II} \end{bmatrix} \begin{Bmatrix} \dot{d}_{D\xi} \\ \dot{d}_{D\eta} \\ \vdots \\ 0 \end{Bmatrix} \quad (\text{Eq 47})$$

### 3. Results and Discussion

#### 3.1 Advanced Model Illustration

Referring to the Appendix and Fig. 6, an ideal work model of linear strain rate variation, which was proposed by Srinivasan et al. (Ref 1), was studied as an example. The results of the present advanced model therefore can be compared with the ideal work model. Figure 7 shows the relation of the nondimensional  $H_1$  to the reduction  $R$ . It is found that the reduction  $R$  has the same value under different  $H_1$  value in the ideal work model. However, it increases with increasing values of  $H_1$  and  $m$  in the advanced model. The discrepancy is also increased with  $H_1$  and  $m$ . The reduction value will approach the ideal work model for the small  $H_1$  in the advanced model. The physical meaning of the  $H_1$  is similar to the  $D$  parameter used in the traditional metal working analysis, which is defined as the ratio of the diameter of the work metal to the contacted length between the tool and work metal. Backofen (Ref 6) and Lo (Ref 7, 8) indicate that the inhomogeneity and hardness variation increase with  $D$  parameter. It is therefore reasonable to see that the answer deviates from the ideal work model for larger  $H_1$  and friction factor  $m$ .

Figure 8 shows the relation between  $R^*$  and  $E$  for  $H_1$  being equal to one in the axisymmetric extrusion. It is found that the nondimensional strain rate  $E$  is smaller for the larger friction factor  $m$  at the same size reduction  $R^*$ . From the definition of  $E$ , it can be seen that, if the same strain rate is assumed in the extrusion, a larger ram velocity is required for the larger friction factor case.

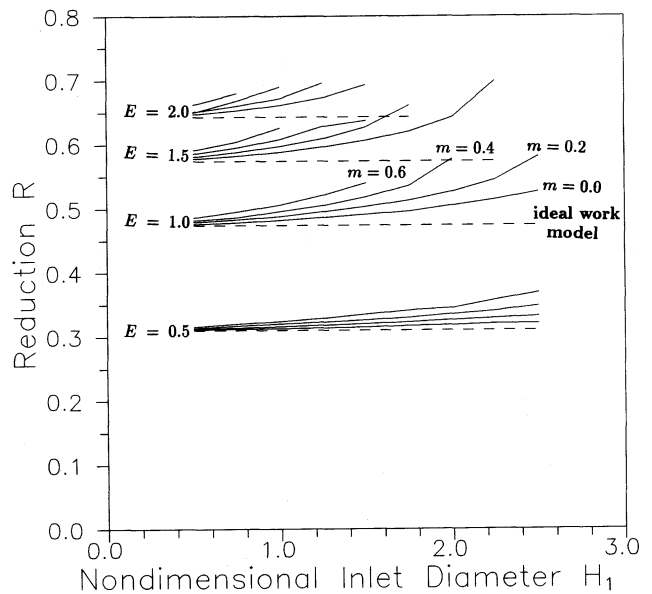


Fig. 7 Relation of reduction with nondimensional inlet diameter  $H_1$

Figure 9 uses a five degree polynomial equation to describe the profile of the dies with  $R^* = 0.4$ . The results from the ideal work model and advanced model are compared. The influence of friction factor  $m$  is also studied. It is noted that although the discrepancy is minor in the figure, the predicted ram velocity from these two models will be quite different for the same prescribed strain rate.

### 3.2 Numerical Illustration

The analysis of the extrusion process was based on the axisymmetric condition. Due to the axisymmetry of the billet, only the upper portion of the die and workpiece were modelled. An automatic mesh was used to generate the finite element mesh, which is comprised of four triangular elements making up a quadrilateral element (Ref 9). Figure 10 shows the initial shape of the die and the finite element mesh of workpiece. The material parameters assumed in the present simulation are (Ref 4):

Stress-Strain Relation:  $\bar{\sigma} = 147.5(0.01 + \epsilon_p)^{41628}$  MPa  
 Friction Factor:  $m = 0.0$  and  $0.4$

The Young's modulus and Poisson's ratio are equal to 69100 MPa and 0.3, respectively. Both of the ideal work and advanced models are investigated in the numerical simulation. The results are compared with each other to verify the developed theory.

Figure 11 shows the resultant strain rate contour of size reduction  $R^* = 0.4$  for two models. It is noted that the nondimensional strain rate  $E$  is equal to  $\dot{\epsilon}L/u_r$ . Hence, the ram velocity  $u_r$  will be different for the ideal work and advanced models. In order to have a good comparison, the strain rate is set as  $\dot{\epsilon} = 4/s$ , and the die length is set at  $L = 1$  mm. Because the  $R^* = 0.4$ , the nondimensional  $E$  will be 1.98 and 1.84 for the ideal work model and frictionless advanced model, respectively. Hence, the velocities for these two models were about to be 2.0 and 2.17 mm/s. The contour lines indicate various strain rate, as

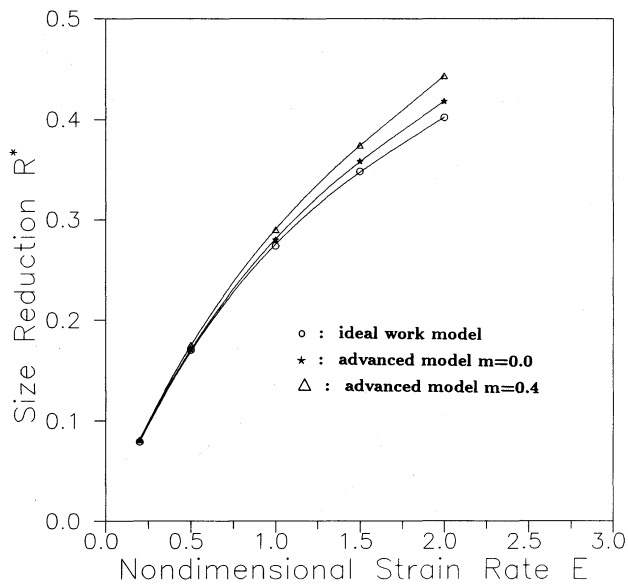


Fig. 8 Relation of size reduction and nondimensional strain rate for  $H_1 = 1$

shown in the figure. It is observed that a substantial portion of strain rate approximately 3.2/s (contours 5) to 4.0/s (contours 6) is in the reduction area of the die for the ideal work model and frictionless advanced model.

It is important to see whether the advanced model is more suitable than the ideal work model in the frictional cases. A friction factor  $m = 0.4$  is used for the ideal work model and advanced model. Figure 12 shows the resultant strain rate contour. A large portion of strain rate, approximately 3.5 to 4.3/s is found in the reduction region for the advanced model. Whereas a smaller portion of strain rate approximately 3.8 to 4.7/s is distributed in the reduction region for the ideal work model. And the maximum strain rate 4.7/s is approximately 9% larger than the advanced model. Hence, the advanced model has a better result in the frictional case.

Figure 13 investigates the influence of the material strain hardening exponent to the strain rate distribution in the advanced frictionless model. The strain hardening exponent varies from 0.4618 to 0.3, 0.2, and 0.1. The maximum strain rate for these three strain parameters are 4.002, 3.971, and 4.08/s, respectively. This result is consistent with the strain hardening exponent and should have no influence in the development of the advanced model theory.

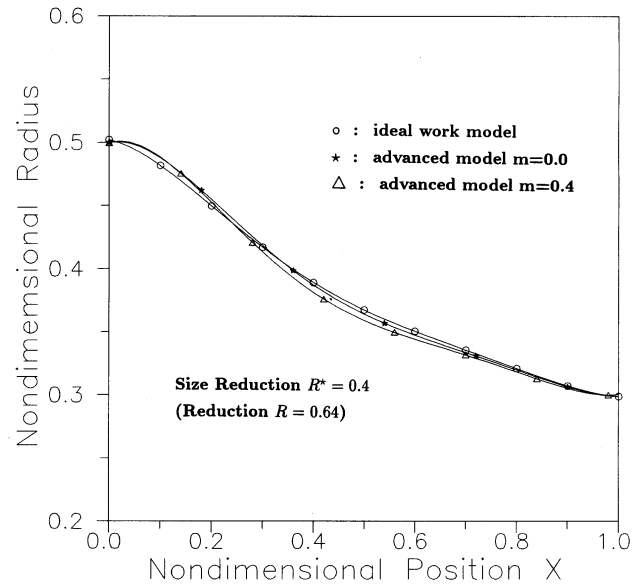


Fig. 9 Die shapes for axisymmetric extrusion with  $H_1 = 1$

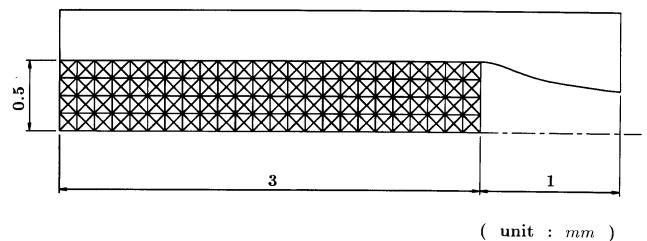
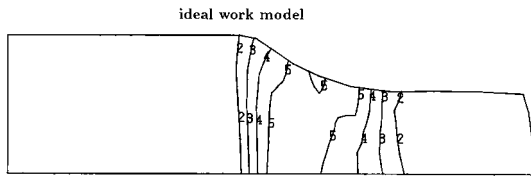


Fig. 10 The initial workpiece and finite element mesh

CONTOUR VALUES

- 1 : 0.009
- 2 : 0.801
- 3 : 1.593
- 4 : 2.385
- 5 : 3.177
- 6 : 3.969



CONTOUR VALUES

- 1 : 0.011
- 2 : 0.824
- 3 : 1.637
- 4 : 2.451
- 5 : 3.264
- 6 : 4.078

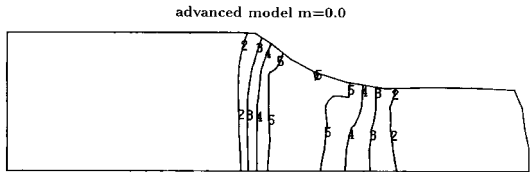
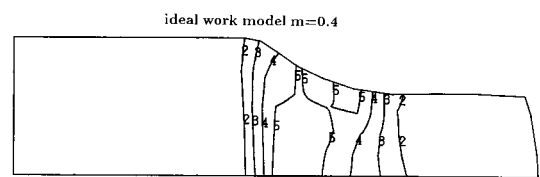


**Fig. 11** Strain rate contour of ideal work and advanced models for  $R^* = 0.4$

CONTOUR VALUES

- 1 : 0.012
- 2 : 0.955
- 3 : 1.898
- 4 : 2.841
- 5 : 3.784
- 6 : 4.728



CONTOUR VALUES

- 1 : 0.007
- 2 : 0.873
- 3 : 1.738
- 4 : 2.604
- 5 : 3.469
- 6 : 4.335

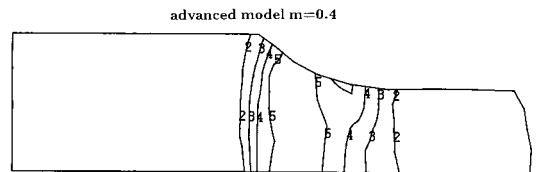
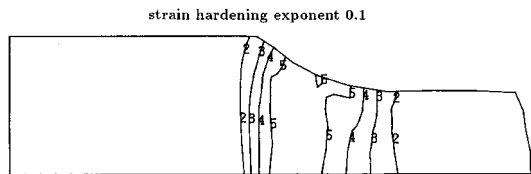


**Fig. 12** Strain rate contour of ideal work and advanced models for  $m = 0.4$

A conveniently explicit form of the load-correction matrix, which is indispensable for the change in configuration of the surface traction rate equilibrium, is derived clearly for the application in the finite element analysis. The friction-correction matrix based on the constant shear friction law along the tool workpiece is also derived to solve interfacial friction. After combining these matrices into the usual elasto-plastic large deformation finite element program, the verification of the advanced model is achieved by comparing the strain rate distribution with the ideal work model. The maximum strain rate will be consistent with each other for the ideal work model and frictionless advanced model. But the advanced model will be better than the ideal work model in the consideration of interfacial friction. A worthy result is that the material strain hardening exponent will not generate significant influence to the maximum strain rate in the advanced model.

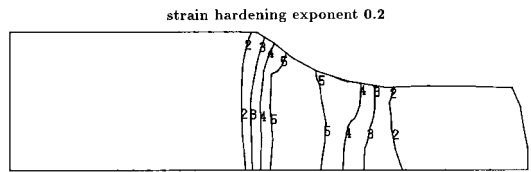
CONTOUR VALUES

- 1 : 0.010
- 2 : 0.824
- 3 : 1.636
- 4 : 2.452
- 5 : 3.266
- 6 : 4.080



CONTOUR VALUES

- 1 : 0.009
- 2 : 0.802
- 3 : 1.594
- 4 : 2.397
- 5 : 3.179
- 6 : 3.971



CONTOUR VALUES

- 1 : 0.009
- 2 : 0.808
- 3 : 1.607
- 4 : 2.405
- 5 : 3.204
- 6 : 4.002

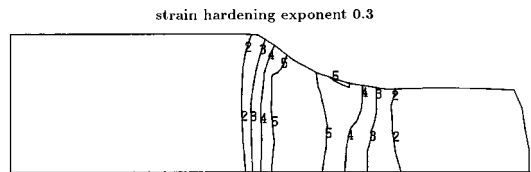


**Fig. 13** Effect of strain hardening exponent to the strain rate contour

### 4. Conclusions

This paper develops an advanced model for the designing of axisymmetric extrusion dies based on a prescribed strain rate. After incorporating the Tresca yield criterion and velocity field with the die angularity, this model can give an accurate prediction of the die shape. The influence of the interfacial friction and the ram velocity are also studied. It is found that not only the ram velocities will be quite different to generate the same controlled strain rate, but also the die shapes are various for the ideal work model and advanced model.

### 5. Appendix

The procedure of designing a controlled strain rate dies based on the ideal work model is described in this section. As the influences of geometric inhomogeneity and friction force on the material flow are ignored, this model gives the preliminary shapes of dies.

Consider an axisymmetric extrusion process as shown in Fig. 1. The die length is  $L$ , and the diameter of the billet is  $h$ . The material undergoes an equivalent strain rate variation as shown in Fig. 6. Consider a slab of material of width,  $dx$ , at a distance,  $x$ , from the entrance to the die. Assuming velocity,  $u$ , and strain rate to be uniform in the slab, the corresponding equivalent strain increment is

$$d\epsilon = -2d\epsilon_r = -2\frac{dh}{h} \quad (\text{Eq 48})$$

The time required to move a distance  $dx$  in the slab is given by

$$dt = dx/u \quad (\text{Eq 49})$$

The equivalent strain rate of the material will be:

$$\dot{\epsilon} = -2\frac{u}{h} \frac{dh}{dx} \quad (\text{Eq 50})$$

Incompressibility is assumed in the process. And  $u_1$  and  $h_1$  are the entrance velocity and the billet diameter, respectively. Then

$$\dot{\epsilon} = -2\frac{u_1 h_1^2}{h^3} \frac{dh}{dx} \quad (\text{Eq 51})$$

Equation 51 can be rewritten in the following form. That is

$$\frac{1}{h^2} = \frac{1}{u_1 h_1^2} \int_{x_1}^x \dot{\epsilon} dx + \frac{1}{h_1^2} \quad (\text{Eq 52})$$

Following the procedure of Srinivasan et al. (Ref 1), a simple strain rate variation is considered described by three straight lines having slopes  $s_1$ ,  $s_2$ , and  $s_3$ , as shown in the figure. The strain rate increases linearly from zero to a constant value then drops to zero near the exit. The condition of zero strain rate at the entrance and exit will generate a smooth die shape and avoid redundant work due to sudden change of geometry. The equivalent strain rate is therefore:

$$\begin{aligned} \dot{\epsilon} &= s_1 x & 0 \leq x \leq L_1 \\ &= s_1 L_1 + s_2 (x - L_1) & L_1 \leq x \leq L_2 \\ &= s_1 L_1 + s_2 (L_2 - L_1) + s_3 (x - L_2) & L_2 \leq x \leq L \end{aligned} \quad (\text{Eq 53})$$

Equations 52 and 53 yield:

$$\frac{1}{h^2} = \frac{s_1 x^2}{2q} + \frac{1}{h_1^2} \quad 0 \leq x \leq L_1 \quad (\text{Eq 54})$$

$$\begin{aligned} \frac{1}{h^2} &= \frac{1}{q} \left[ \frac{s_2 - s_1}{2} L_1^2 + (s_1 - s_2) L_1 x + s_2 \frac{x^2}{2} \right] + \frac{1}{h_1^2} \\ &L_1 \leq x \leq L_2 \end{aligned} \quad (\text{Eq 55})$$

and

$$\begin{aligned} \frac{1}{h^2} &= \\ &\frac{1}{q} \left[ \frac{s_2 - s_1}{2} L_1^2 + \frac{s_3 - s_2}{2} L_2^2 + (s_1 - s_2) L_1 x + (s_2 - s_3) L_2 x + s_3 \frac{x^2}{2} \right] \\ &+ \frac{1}{h_1^2} \quad L_2 \leq x \leq L \end{aligned} \quad (\text{Eq 56})$$

where  $q$  is the volume flow rate, which equals  $u_1 h_1^2$ . In addition,  $h$  is equal to  $h_2$  at the exit, which yields:

$$\frac{1}{1 - R} = 1 + \frac{g}{u_1} \quad (\text{Eq 57})$$

where

$$\begin{aligned} g &= \frac{s_2 - s_1}{2} L_1^2 + \frac{s_3 - s_2}{2} L_2^2 + (s_1 - s_2) L_1 L + (s_2 - s_3) L_2 L \\ &+ s_3 \frac{L^2}{2} \end{aligned} \quad (\text{Eq 58})$$

and  $R$  is the reduction defined as

$$R = 1 - (h_2/h_1)^2 \quad (\text{Eq 59})$$

For a special case with constant strain rate,  $s_2 = 0$ , the non-dimensional strain rate,  $E$ , can be defined as:

$$E = \dot{\epsilon} L / u_1 = s_1 L_1 L / u_1 \quad (\text{Eq 60})$$

and two factors

$$f_1 = L_1 / L \quad (\text{Eq 61})$$

and

$$f_2 = L_2 / L \quad (\text{Eq 62})$$

Then the reduction  $R$  can be expressed in terms of these factors and  $E$ :

$$R = 1 - [1 + (1 - f_1 + f_2)E/2]^{-1} \quad (\text{Eq 63})$$

It can be seen from Eq 60 and 63 that for a given constant strain rate and fixed  $f_1$  and  $f_2$ , the reduction  $R$  is unchanged if  $u_1/L$  is constant. And the ratio of the entrance diameter  $h_1$  to the die length  $L$ :

$$H_1 = h_1 / L \quad (\text{Eq 64})$$

however, is independent of  $R$ . This is not reasonable for large values of  $H_1$ . In addition, the friction force on the die-work-piece interface also has a significant influence on  $R$  for large  $E$  and  $H_1$ .

## References

1. R. Srinivasan, J.S. Gunasekera, H.L. Gegel, and S.M. Doraivelu, Extrusion Through Controlled Strain Rate Dies, *J. Mater. Shaping Technol.*, Vol 8 (No. 2), p 133-141
2. D.F. Chang, "An Advanced Slab Analysis of the Strip Rolling Process," Ph.D. dissertation, Northwestern University, 1994
3. Y.M. Huang, Y.H. Lu, T. Hirakawa, and Y. Yamada, The Elasto-Plastic Analysis of Close-Pass Drawing of Tube with Moving

- Mandrel, *Proc. Third Conf. Steel Rolling* (Tokyo, Japan), 1985, p 513-520
4. Y.M. Huang, Y.H. Lu, and J.W. Chan, "An Elasto-Plastic Finite Element and Experimental Study of the Ironing Process," *J. Mater. Process. Technol.*, Vol 26, 1991, p 53-80
  5. Y. Yamada, Nonlinear Matrices, Their Implications and Applications in Inelastic Large Deformation Analysis, *Comput. Meth. Appl. Mech. Eng.*, Vol 33 (No. 1), 1982, p 417-437
  6. W.A. Backofen, *Deformation Processing*, Addison-Wesley, 1972, p 140
  7. S.W. Lo, An Efficient Method of Designing Controlled Strain Rate Dies for Extrusions, *J. Chin. Inst. Eng.*, Vol 19 (No. 5), 1996, p 1-9
  8. S.W. Lo, Preliminary Die Design for Extrusion of Compressible Porous Materials, *Chin. J. Mech.*, Vol 12 (No. 3), 1996, p 353-362
  9. J.C. Nagtegaal, D.M. Parks, and J.R. Rice, On Numerically Accurate Finite Element Solutions in Fully Plastic Range, *Comput. Meth. Appl. Mech. Eng.*, Vol 4 (No. 2), 1974, p 153-177